

Theoretical study of the pressure-induced structure, phase transition, mechanical and electronic properties in the V-N system

Jin Zhang,^{1,*} Xinfeng Li,² Xiao Dong,³ Huafeng Dong,⁴ and Artem R. Oganov^{5,6,7,†}

¹*Department of Geosciences, Center for Materials by Design, and Institute for Advanced Computational Science, State University of New York, Stony Brook, NY 11794-2100, USA*

²*Sino-French Institute of Nuclear Engineering and Technology, Sun Yat-sen University, Zhuhai, Guangzhou 519082, China*

³*Key Laboratory of Weak-Light Nonlinear Photonics and School of Physics, Nankai University, Tianjin 300071, China*

⁴*School of Physics and Optoelectronic Engineering,*

Guangdong University of Technology, Guangzhou 510006, China

⁵*Skolkovo Institute of Science and Technology, Skolkovo Innovation Center, 3 Nobel St., Moscow, 143026, Russia*

⁶*Moscow Institute of Physics and Technology, 9 Institutskiy Lane, Dolgoprudny 141700, Russia*

⁷*International Center for Materials Discovery, Northwestern Polytechnical University, Xi'an, Shaanxi 710072, PR China*

Stable compounds in the V-N system are systematically searched and four new high-pressure phases are found, including $C2/m$ -V₉N, $Pbam$ -V₅N₂, $Pnma$ -V₂N and $I4/mcm$ -VN₂. V₂N undergoes a phase transition from ϵ -Fe₂N-type V₂N ($P\bar{3}1m$) to ζ -Fe₂N-type V₂N ($Pbcn$) at 10 GPa and to Fe₂C-type V₂N ($Pnmm$) at 59 GPa, then to $Pnma$ -V₂N at 96 GPa. Low-temperature tetragonal VN is theoretically proved to belong to space group $P42m$. The estimated Vickers hardnesses and fracture toughness of WC-type VN are around 37 GPa and 4.3-6.1 MPa m^{1/2}, respectively. Al₂Cu-type VN₂ ($I4/mcm$) with a Vickers hardness of 25-27 GPa and fracture toughness of 3.6-6.6 MPa m^{1/2} also shows excellent mechanical properties. Elastic properties of WC-type mononitrides of transition metals from IVB group (Ti, Zr and Hf), VB group (V, Nb and Ta) and VIB (Cr, Mo and W) are calculated and compared. Both the bond strength and structural configuration determine the mechanical properties of a material.

I. INTRODUCTION

Compared with pure metals, transition metal nitrides have extremely strong and short bonds which lead to a very low compressibility and high hardness. Therefore, a great deal of work has been performed to the search for new transition metal nitrides (and also carbides and borides) with extreme hardness and good fracture toughness, in the hope that many of these will find applications in cutting tools and as hard coatings. Among these metal nitrides, vanadium nitride becomes an attractive candidate because of its high hardness^{1,2}, high melting point³, good corrosion resistance⁴ and low friction coefficient^{5,6}. Based on the combination of these outstanding physical and chemical properties, vanadium nitride thin films have been fabricated to be used as hard coatings^{7,8} and nanocrystalline vanadium nitride can become an attractive material for supercapacitors⁹.

Properties are closely related to the structure of materials. For the crystal structures of V-N compounds, it has been established that β -V₂N_{1-x} has a ϵ -Fe₂N-type ($P\bar{3}1m$ -V₂N) structure and δ -VN_{1-x} has a NaCl-type ($Fm\bar{3}m$ -VN)¹⁰. δ' -VN_{1-x} (V₃₂N₂₆) was reported to exist below 520 °C and the lattice constant of its structure is twice as large as that of the original NaCl-type cell with six nitrogen atoms removed from the unit cell¹¹. In addition, three metastable phases with stoichiometries V₁₆N, V₈N and V₉N₂ have been reported^{12,13} and can be formed according to a proposed metastable phase diagram¹⁰. Other intermediate phases, including V₁₃N, V₉N and V₄N are believed to metastably exist¹³.

Much effort has been made to explore the structures of these stable or metastable vanadium nitrides. Even for the simple vanadium mononitride, a significant amount of attention has been paid to study its crystal structure. Three decades ago, Kubel's¹⁴ experiment detected that VN crystallizes in the NaCl-type structure at 298 K and transforms into a low-temperature tetragonal-VN (a distorted NaCl-type phase, space group: $P42m$) at 205 K. Afterward, Weber's inelastic neutron scattering experiment¹⁵ found that NaCl-type VN exhibits a notably soft mode in its acoustic branch at room temperature. Meanwhile, first-principles calculations showed that NaCl-type VN is dynamically unstable according to its phonon dispersion curves^{16,17} and also indicated that WC-type VN ($P\bar{6}m2$ -VN) has the lowest energy at zero pressure¹⁸⁻²⁰. To explore the reason that NaCl-type VN is experimentally detected at room temperature while it is dynamically unstable from the first-principles calculation at 0 K. Ivashchenko's density functional theory (DFT) calculation¹⁹ proposed that vacancies stabilize NaCl-type VN compared to WC-type VN. Mei²¹, by performing both experiment and *ab initio* molecular dynamics, found that tetragonal-VN appeared below 250 K and NaCl-type VN was thermodynamically stabilized by the temperature-induced anharmonic effects.

However, despite abundant theoretical and experimental studies of V-N compounds, less information is provided on the pressure-induced new compounds in the V-N system. Moreover, except that the hardness of bulk $Fm\bar{3}m$ -VN (13 GPa) is reported by previous experiments^{22,23}, the mechanical properties of other V-N

compounds are still experimentally lacking due to the difficulty of preparing the samples with different stoichiometries. In this work, we perform a comprehensive calculation to investigate the V-N system at pressure up to 120 GPa, analyze the dynamical stability of high-pressure phases, calculate the elastic constants of these high-pressure phases and then predict their hardness and fracture toughness at 0 GPa. Indeed, several new stoichiometries in the V-N system have been predicted under high pressure and they were found to possess unusual mechanical properties.

II. COMPUTATIONAL METHODOLOGY

Stable phases in the V-N system were searched using first-principles evolutionary algorithm (EA) as implemented in the USPEX code^{24–26} combined with *ab initio* structure relaxations using DFT with the Perdew–Burke–Ernzerhof (PBE) generalized gradient approximation (GGA) exchange–correlation functional²⁷, as implemented in the VASP package²⁸. We also tested the DFT+U method, but the calculated enthalpies of formation from pure DFT agree better with the experimental data at 0 K from NIST-JANAF thermochemical tables²⁹. The variable-composition structure searches²⁶ were performed for the V-N system at 0 GPa, 10 GPa, 20 GPa, 30 GPa, 40 GPa, 50 GPa, 60 GPa, 70 GPa, 80 GPa, 90 GPa, 100 GPa, 110 GPa and 120 GPa. Several fixed-composition searches were also performed for vanadium mononitride at 0 GPa and for low-enthalpy metastable compounds found at various pressures. The initial generation of structures was produced randomly using space group symmetry, each subsequent generation was obtained by variation operators including heredity (40%), lattice mutation (20%), random generator (20%) and transmutation (20%). The electron-ion interaction was described by the projector-augmented wave (PAW) potentials³⁰, with $3p^64s^13d^4$ and $2s^22p^3$ shells treated as valence for V and N, respectively. The plane-wave energy cutoff was chosen as 600 eV and Γ -centered uniform k -meshes with resolution $2\pi \times 0.06 \text{ \AA}^{-1}$ were used to sample the Brillouin zone. Phonon dispersions were calculated using the finite-displacement method implemented in the Phonopy code³¹, based on the Hellmann-Feynman forces calculated with the VASP code. Voigt-Reuss-Hill approximation has been adopted to estimate the polycrystal bulk modulus (B), and shear modulus (G). The Vickers hardness was estimated according to the Chen-Niu’s hardness model³² and its modification by Tian³³, as well as Mazhnik’s hardness model³⁴. The fracture toughness was evaluated by Niu’s fracture toughness model of covalent and ionic crystals³⁵ and Mazhnik’s fracture toughness model³⁴. The calculation of crystal orbital Hamilton population (COHP) was performed using the TB-LMTO-ASA program³⁶ based on the binding linear muffin-tin orbital method with the atomic sphere approximation.

III. RESULTS AND DISCUSSIONS

A. Crystal structure prediction for V-N system

The pressure-composition phase diagram of the V-N system, shown in Fig. 2, was constructed according to the calculated convex-hull diagrams [Fig.1]. Three compounds, $C2/m$ - V_9N , $P\bar{3}1m$ - V_2N and $P\bar{6}m2$ - VN , are stable at zero pressure. Three new compounds are found under high pressure: $I4/mcm$ - VN_2 (Al_2Cu -type) appears at 33 GPa and is stable at least up to 120 GPa; $Pb\bar{a}m$ - V_5N_2 becomes stable at 84 GPa; $Pnma$ - V_2N is a new high-pressure phase of V_2N . The dynamical stabilities of all the V-N compounds were checked by calculating phonon dispersions [Fig. 3], no imaginary vibrational frequencies are found in the whole Brillouin zone at 0 GPa, indicating all these high-pressure vanadium nitrides can be theoretically preserved as metastable phases at ambient pressure.

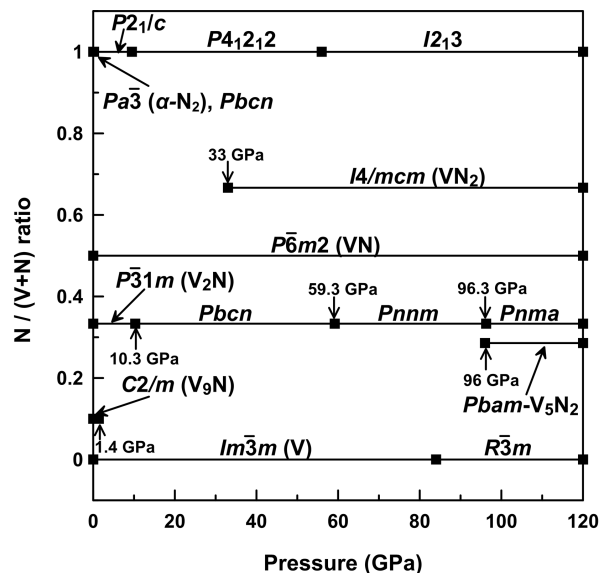


FIG. 2: Pressure-composition phase diagram of the V-N system at pressures up to 120 GPa.

In 1949, ϵ - Fe_2N -type ($P\bar{3}1m$) V_2N structure was proposed by Hahn³⁷ and verified by neutron diffraction of melting vanadium nitride in nitrogen at 1 MPa³⁸. Recently, Ravi¹⁸ performed DFT calculation to study the property and phase stability of ζ - Fe_2N -type V_2N ($Pbcn$), Fe_2C -type V_2N ($Pnnm$) and CdI_2 -type V_2N ($P\bar{3}m1$). Our calculated results show that both ζ - Fe_2N -type and Fe_2C -type V_2N are actually the high-pressure phases of V_2N and V_2N undergoes a series of structural transformation with increasing pressure: ϵ - Fe_2N -type V_2N first transforms into the ζ - Fe_2N -type V_2N at 10 GPa, then to

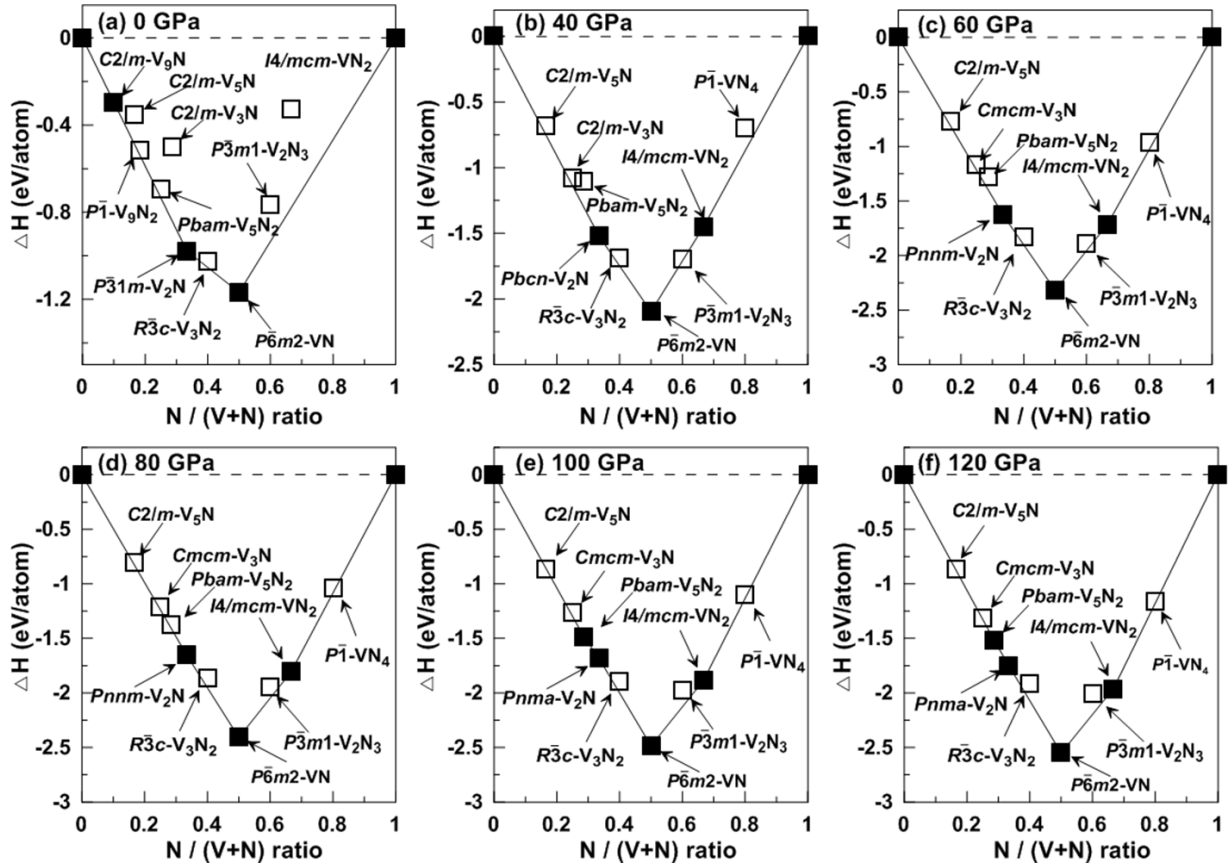


FIG. 1: Convex-hull diagrams for the V–N system at (a) 0 GPa, (b) 40 GPa, (c) 60 GPa, (d) 80 GPa, (e) 100 GPa, and (f) 120 GPa, respectively. Solid squares denote stable phases while open squares represent metastable compounds.

Fe_2C -type- V_2N at 59 GPa, and then to the Pnma - V_2N at 96 GPa, as displayed in Fig. 4. In the ε - Fe_2N -type V_2N , ζ - Fe_2N -type V_2N and Fe_2C -type V_2N structures, all the V atoms are three-coordinate and N atoms are six-coordinate while the coordination numbers of V and N atoms in Pnma - V_2N increase to four and eight, respectively.

Previous experimental studies reported that the NaCl-type VN transforms into a tetragonal VN on cooling and the transition temperature is 204 K for bulk polycrystalline VN samples¹⁴ and 250-300 K for VN films²¹. In our calculations, besides the known WC-type VN ($\text{P}\bar{6}m2$), NiAs-type VN ($\text{P}6_3/mmc$), NaCl-type VN ($\text{Fm}\bar{3}m$) and CsCl-type VN ($\text{Pm}\bar{3}m$), we also successfully found the $\text{P}\bar{4}2m$ -VN which was proposed by Kubel¹⁴; the $\text{P}4_2mc$ -VN and $\text{I}4_1md$ -VN which were reported by Pu's first-principles calculation³⁹; the $\text{P}4_2/mcm$ -VN, and $\text{P}4/nmm$ -VN that were predicted in Ivashchenko's first-principles study¹⁷. Furthermore, new low-energy phases: $\text{R}\bar{3}m$ -VN, $\text{Imm}2$ -VN and $\text{Cmc}2_1$ -VN

were also found. Except NaCl-type VN, which is dynamically unstable at zero pressure and temperature based on the theoretical analysis of its lattice dynamics¹⁶, the dynamical stabilities of all the other vanadium mononitride were checked by calculating phonon dispersions (see Fig. S1 in the Supplementary Materials) at 0 GPa. The results show that the imaginary frequencies are found in phonon dispersion curves of $\text{R}\bar{3}m$ -VN, $\text{P}4/nmm$ -VN and CsCl-type VN, indicating these three structures are dynamically unstable. Then the zero-point energies (ZPE) were calculated for the dynamically stable structures (see relative enthalpy+ZPE values in Table I). Total enthalpy sequence (including ZPE) for the eight dynamically stable structures is WC-type VN < $\text{P}4_2mc$ -VN < $\text{I}4_1md$ -VN < AsNi-type VN < $\text{Imm}2$ -VN < $\text{Cmc}2_1$ -VN < $\text{P}\bar{4}2m$ -VN < $\text{P}4_2/mcm$ -VN. Among them, $\text{P}4_2mc$ -VN, $\text{I}4_1md$ -VN, $\text{P}\bar{4}2m$ -VN and $\text{P}4_2/mcm$ -VN all belong to tetragonal system. From the viewpoint of energetic stability, it seems that $\text{P}4_2mc$ -VN is more promising than experimentally proposed $\text{P}\bar{4}2m$ -VN to be that tetragonal-VN. Is this really the case?

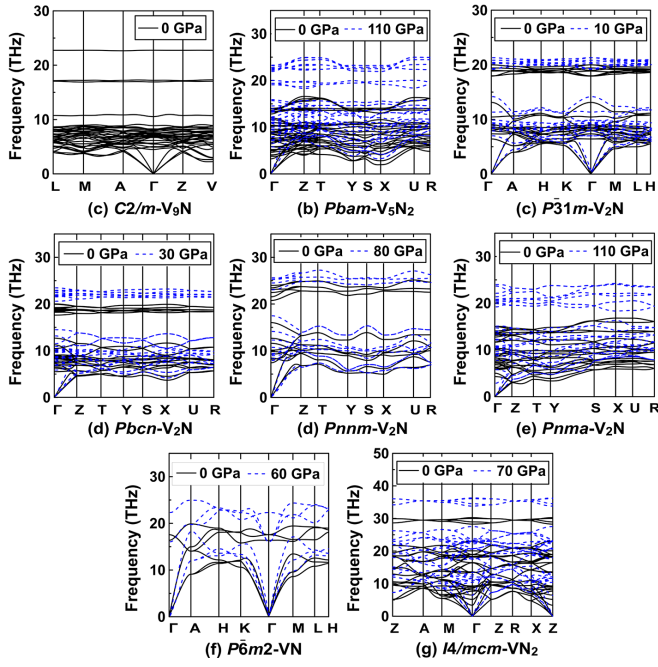


FIG. 3: (Color online) Calculated phonon dispersion curves of V-N compounds along high-symmetry directions of the Brillouin zone. The solid black and dashed blue lines represent the results at zero and high pressures, respectively.

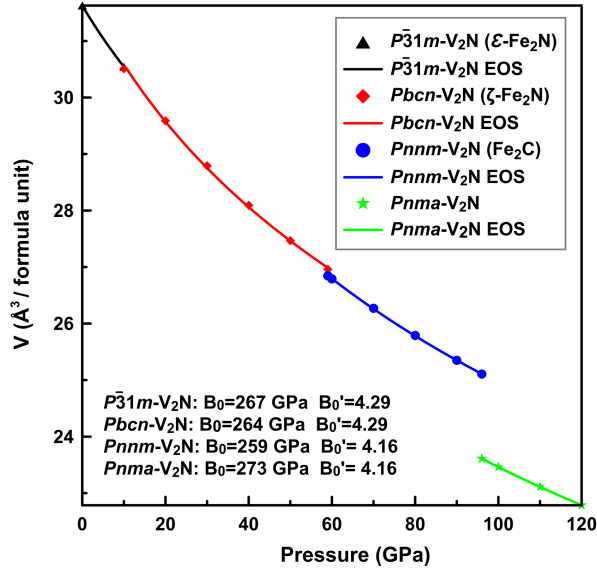


FIG. 4: (Color online) Equation of state (EOS) of V_2N up to 120 GPa. The calculated pressure-volume data were fit with a third-order Birch-Murnaghan equation of state $P(V) = (3B_0/2)[(V/V_0)^{-7/3} - (V/V_0)^{-5/3}]\{1 + (3/4)(B'_0 - 4)[(V/V_0)^{-2/3} - 1]\}$ to find B_0 and B'_0 .

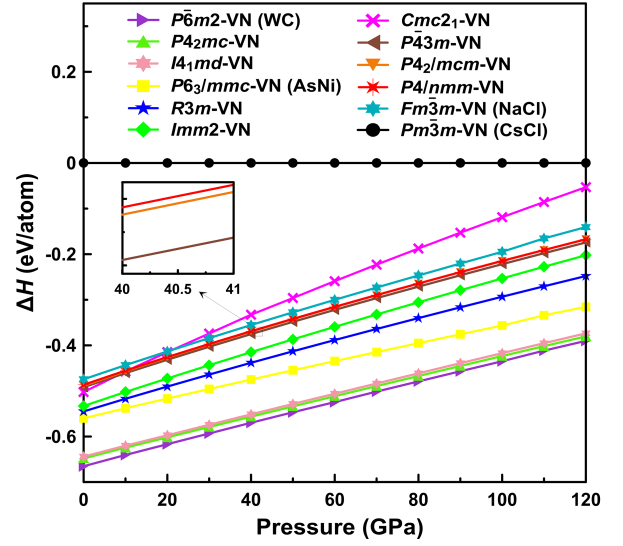


FIG. 5: (Color online) Relative enthalpy as a function of pressure for vanadium mononitrides. CsCl-type VN is taken as reference.

TABLE I: Relative enthalpy (taking the enthalpy of $P\bar{6}m2$ -VN as reference) without and with zero-point energy (ZPE), dynamical stability (DS) for low-energy vanadium mononitrides at 0 GPa. ZPE can only be calculated for the dynamically stable phases. ΔE denotes the relative enthalpy without ZPE and ΔE^* represents the relative enthalpy with ZPE. \checkmark = dynamical stability; \times = dynamical instability; NA = not available.

Compound	ΔE (eV/atom)	DS	ΔE^* (eV/atom)
$P\bar{6}m2$ -VN	0	\checkmark	0
$P4_2mc$ -VN	0.01843	\checkmark	0.00097
$I4_1md$ -VN	0.02239	\checkmark	0.00518
$P6_3/mmc$ -VN	0.10445	\checkmark	0.08094
$R3m$ -VN	0.12156	\times	NA
$Imm2$ -VN	0.13347	\checkmark	0.10848
$Cmc2_1$ -VN	0.16409	\checkmark	0.13914
$P\bar{4}2m$ -VN	0.17469	\checkmark	0.13714
$P4_2/mcm$ -VN	0.17505	\checkmark	0.13846
$P4/nmm$ -VN	0.18003	\times	NA
$Fm\bar{3}m$ -VN	0.19205	\times	NA
$Pm\bar{3}m$ -VN	0.67864	\times	NA

To make this question clear, the selected-area electron diffraction patterns of tetragonal vanadium mononitrides ($P4_2mc$ -VN, $I4_1md$ -VN, $P\bar{4}2m$ -VN, $P4_2/mcm$ -VN and $P4/nmm$ -VN) were calculated using CrystalMaker software⁴⁰. It turns out that only the calculated selected-area electron diffraction patterns of $P\bar{4}2m$ -VN perfectly match the experimental electron diffraction of tetragonal-VN²¹, see the Fig. S4 in Supplementary Materials. Therefore, we can confirm that the experimentally observed tetragonal-VN is $P\bar{4}2m$ -VN. Nevertheless, why

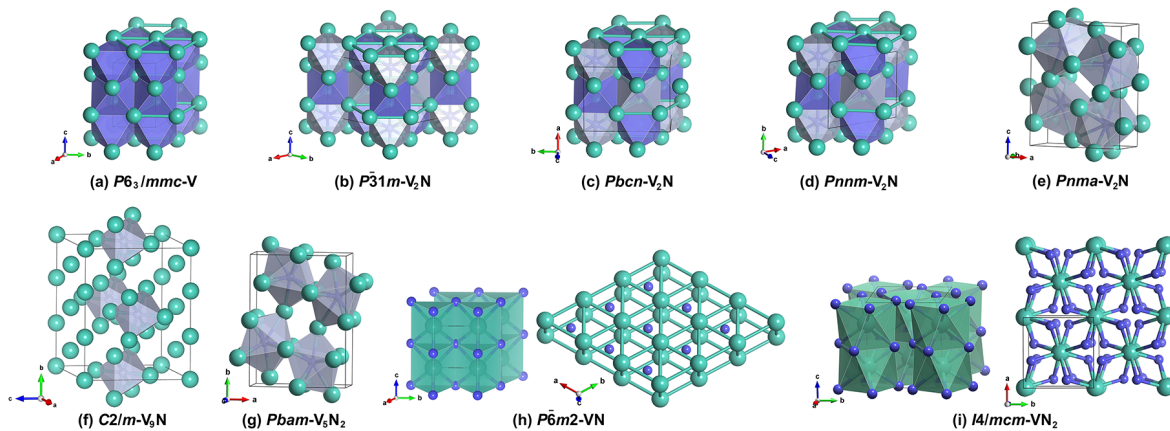


FIG. 6: (Color online) Crystal structures of (a) $P6_3/mmc-V$; (b) $P\bar{3}1m-V_2N$; (c) $Pbcn-V_2N$; (d) $Pnnm-V_2N$; (e) $Pnma-V_2N$; (f) $C2/m-V_9N$; (g) $Pbam-V_5N_2$; (h) $P\bar{6}m2-VN$; (i) $I4/mcm-VN_2$. The hcp sublattices of vanadium are highlighted in polyhedral representation of (a), (b), (c) and (d). Nitrogen-centered octahedra and nitrogen vacancies are shown as light and dark purple polyhedra, respectively. Vanadium-centered polyhedra are shown in green.

the tetragonal-VN is identical to $P\bar{4}2m-VN$, and not to the more energetically favorable tetragonal $P4_2mc-VN$ or $I4_1md-VN$? The most probable reason is the strong anharmonicity of VN²¹. The enthalpy-pressure diagram (without ZPE) of vanadium mononitrides is drawn in Fig. 5. WC-type VN structure, which was never reported by the experiment, might be synthesized through the application of pressure.

B. Structures of V-N compounds

The optimized structural parameters for V-N compounds are listed in Table S1 in Supplementary Materials. $C2/m-V_9N$ and $Pbam-V_5N_2$, which respectively have six-coordinate N and eight-coordinate N in their structures, cannot be derived from close packing. The hexagonal structure of WC-type VN has V atoms in a sixfold trigonal prismatic coordination, as displayed in Fig. 6(h).

$P\bar{3}1m-V_2N$, $Pbcn-V_2N$ and $Pnnm-V_2N$ are formed by nitrogen atoms occupying the octahedral interstitial sites of hcp vanadium sublattice. The polyhedral representations of these V_2N structures are shown in Fig. 6(b) (c) (d) and hcp vanadium [Fig. 6(a)] is drawn for comparison. The structure of $P\bar{3}1m-V_2N$ also derives from hcp vanadium, in which nitrogen atoms occupy the octahedral interstitial sites. Close-packed vanadium sublattice is no longer observed in the higher-pressure phase $Pnma-V_2N$ [see Fig. 6(e)].

The crystal structure of high-pressure VN₂ phase is similar with that of high-pressure TiN₂⁴¹. Both of them have the Al₂Cu-type ($I4/mcm$) structure. This is different with the case in transition metal borides where the Al₂Cu-type structure is often formed with a transition metal /boron ratio of 2:1 (e.g. Ti₂B, Cr₂B, Mn₂B, Fe₂B, Co₂B, Ni₂B and Mo₂B)⁴² while the AlB₂-type

($P6/mmm$) structure is predominant for transition metal borides with a transition metal/boron ratio of 1:2 (e.g. TiB₂, VB₂, CrB₂, MnB₂, FeB₂, MoB₂, IrB₂)^{43,44}.

C. Mechanical properties of V-N compounds

The elastic moduli, including bulk modulus B , shear modulus G and Young's modulus E of V-N compounds are calculated from the elastic tensors, and theoretical hardnesses and fracture toughness [listed in Table II] can be further predicted based on the empirical models³²⁻³⁵. All the V-N compounds have high bulk moduli. The mechanical stabilities of the vanadium nitrides have been checked by calculating their elastic constants and all these compounds are mechanically stable at 0 GPa based on the Born criteria of mechanical stability⁴⁵.

Fracture toughness describes the resistance of a material against crack propagation and is one of the most critical mechanical properties of materials. Design of a material with excellent mechanical properties requires both high hardness and high fracture toughness. WC-type VN possess the best combination of hardness (~ 37 GPa) and fracture toughness (4.3-6.1 MPa m^{1/2}). The second hardest V-N compound is $I4/mcm-VN_2$ which also has good fracture toughness with the value of 3.6-6.6 MPa m^{1/2}. $C2/m-V_9N$ exhibits poor fracture toughness and its hardness is around 3.5-9.8 GPa.

Poisson's ratio ν correlates with the degree of metallicity: the higher value of ν , the weaker covalent bonding in the structure, the more metallic the material, and the lower hardness of this material⁴⁸. Superhard phases generally have a low Poisson's ratio (about 0-0.2)⁴⁹. This is in accordance with our calculated Poisson's ratio for V-N compounds (Table II), e.g. WC-type VN and $I4/mcm-VN_2$, which exhibit higher hardness, have low Poisson's ratios 0.18 and 0.22, respectively. Large values of C_{33}

TABLE II: Calculated bulk modulus B , shear modulus G , Young's modulus E , Poisson's ratio ν , volume per atom V_0 , Vickers hardness H_v (H_v^c is calculated from Chen-Niu's model, H_v^t is calculated from Tian's modification model³³, H_v^m is calculated from Mazhnik's model³⁴) and fracture toughness K_{IC} (K_{IC}^n is calculated from Niu's model³⁵, K_{IC}^m is calculated from Mazhnik's model³⁴) of V-N compounds at 0 GPa, as well as literature values for $Fm\bar{3}m$ -VN. G/B and ν are dimensionless; K_{IC} is in MPa m^{1/2}; V_0 is in $\text{\AA}^3/\text{atom}$. Hardness, B , G and E are in GPa.

Compound	C_{11}	C_{22}	C_{33}	C_{44}	C_{55}	C_{66}	C_{12}	C_{13}	C_{14}	C_{16}	C_{23}	C_{26}	C_{36}	B_H	G_H	E	G/B	ν	V_0	H_v^c	H_v^t	H_v^m	K_{IC}^n	K_{IC}^m
$C2/m$ -V ₉ N	278	314	282	49	55	87	130	166		-7		-3	-1	193	65	176	0.34	0.35	12.72	3.5	5.2	9.8	1.7	2.8
$Pbam$ -V ₅ N ₂	351	400	417	153	117	93	197	169			189			252	111	291	0.44	0.31	10.25	9.1	10.2	15.4	2.5	4.3
$P\bar{3}1m$ -V ₂ N	453		441	149			162	182	26					267	142	361	0.53	0.27	10.54	14.3	14.9	17.7	2.9	4.7
$Pbcn$ -V ₂ N	424	465	459	147	158	155	180	176			157			264	147	372	0.56	0.26	10.53	15.7	16.2	17.8	2.9	5.0
$Pnmm$ -V ₂ N	473	419	472	145	148	180	171	147			157			257	153	383	0.60	0.25	10.52	17.7	18.0	17.8	2.9	4.4
$Pnma$ -V ₂ N	385	450	457	153	129	130	208	188			160			267	130	335	0.49	0.29	9.82	11.9	12.7	17.1	2.7	4.7
$P\bar{6}m2$ -VN	634		890	271			172	127						332	267	631	0.80	0.18	8.65	37.6	37.4	37.7	4.3	6.1
$Fm\bar{3}m$ -VN	621			119			162							315	156	401	0.49	0.29	8.77	13.8	14.7	20.3	3.2	5.6
	616 ^a			165 ^a			163 ^a							312 ^a	156 ^a	402 ^a		0.29 ^a		10-13 ^{b,c}				
$P\bar{4}2m$ -VN	510		510	127		127	198	198						302	138	360	0.46	0.30	8.77	11.3	12.4	18.8	2.9	5.1
$I4/mcm$ -VN ₂	631		609	168		292	212	127						311	214	522	0.69	0.22	7.71	26.8	26.9	24.8	3.6	6.6

^aCalculated GGA result⁴⁶, ^bExperiment²², ^cExperiment⁴⁷.

(890 GPa) and C_{44} (271 GPa) for WC-type VN indicate its extremely high incompressibility along the c-axis and great resistance to shear deformation. Pugh proposed a modulus ratio (G/B ratio) to discriminate between brittle and ductile phases⁵⁰: a material is deemed to be brittle if $G/B > 0.57$ and $G/B < 0.57$ indicates a ductile material. Hence, WC-type VN, $I4/mcm$ -VN₂ and $Pnmm$ -V₂N are brittle while $Pbam$ -V₅N₂, $P\bar{3}1m$ -V₂N, $Pbcn$ -V₂N and $Pnma$ -V₂N are ductile.

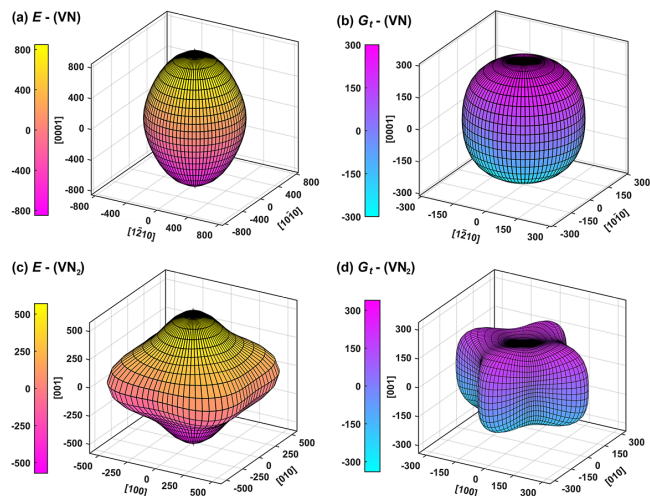


FIG. 7: (Color online) Illustration of direction dependent of Young's modulus E and torsion modulus G_t for $P\bar{6}m2$ -VN and $I4/mcm$ -VN₂.

Given that WC-type VN exhibits remarkable elastic moduli, it is natural to consider if these outstanding mechanical properties would be found in other WC-type transition metal (TM) mononitrides. Here, we computed elastic moduli, hardnesses and fracture toughness of nitro compounds combined with transitional elements from IVB,

VB and VIB groups [see Table III]. The result indicates that group VB mononitrides exhibit higher hardness and fracture toughness. Bulk moduli increase from IVB to VB to VIB mononitrides, whereas shear moduli peak at VB mononitrides.

All the crystals are elastically anisotropic, which can be favourable for the emergence of microcracks⁵⁹. Calculating and visualizing the elastic anisotropy is important for understanding these properties and optimizing them for practical applications. The directional dependence of Young's modulus (E) and torsion shear modulus (G_t) for the two hardest V-N compounds (WC-type VN and $I4/mcm$ -VN₂) is displayed in Fig. 7. A surface construction can be used to clearly reflect the variation of Young's modulus and torsion shear modulus, while it is impossible to represent the direction-dependent shear modulus by three-dimensional diagrams since it is not only related to the direction of the shear plane but also related to the direction of the force. Therefore in engineering, the torsion shear modulus (G_t , an average in the shear plane), which can be represented by three-dimensional diagrams, is used for visualizing the anisotropy of a material. For an isotropic system, one would see a spherical shape. The degree of elastic anisotropy in a system can be directly extracted from asphericity of these figures. The magnitudes of anisotropy of Young's modulus (E) and torsion shear modulus (G_t) for $I4/mcm$ -VN₂ are greater than that of WC-type VN.

D. Electronic structure and chemical bonding of V-N compounds

Total and projected density of states (DOS) of V-N compounds are presented in Fig. 8. All the V-N compounds exhibit metallic behavior and a hybridization be-

TABLE III: Calculated bulk modulus B , shear modulus G and hardness of WC-type structures for nitrogen combined with transitional elements from IVB (Ti, Zr and Hf), VB (V, Nb and Ta) and VIB (Cr, Mo and W) groups at 0 GPa. Except dimensionless G/B and K_{IC} in MPa $m^{1/2}$, all properties are in GPa. Superscript * represents the structure is the metastable phase while + represents the structure is the stable structure at zero pressure and temperature at the GGA level. H_v^c is calculated from Chen-Niu's model, H_v^t is calculated from Tian's modification model³³, H_v^m is calculated from Mazhnik's model³⁴, K_{IC}^n is calculated from Niu's model³⁵ and K_{IC}^m is calculated from Mazhnik's model³⁴. Note the most stable structure for NbN is anti-WC-type structure instead of WC-type structure^{51,52}, thus the superscript * is used for WC-type NbN in this table.

Compound	B_H	G_H	G/B	H_v^c	H_v^t	H_v^m	K_{IC}^n	K_{IC}^m	Compound	B_H	G_H	G/B	H_v^c	H_v^t	H_v^m	K_{IC}^n	K_{IC}^m	Compound	B_H	G_H	G/B	H_v^c	H_v^t	H_v^m	K_{IC}^n	K_{IC}^m
TiN*	257	148	0.58	16.5	16.9	17.6	2.9	3.6	VN*	332	267	0.8	37.6	37.4	37.7	4.3	6.1	CrN*	354	227	0.64	25.4	25.9	25.8	4.0	5.8
ZrN*	222	116	0.52	12.0	12.7	14.7	2.5	2.9	NbN*	312	217	0.70	27.5	27.6	25.4	3.9	5.3	MoN*	347	153	0.44	11.5	12.8	21.2	3.4	5.0
	225 ^d	118 ^d	0.52 ^d							316 ^d	209 ^d	0.66 ^d							351 ^d	181 ^d	0.52 ^d					
															345 ^c											
HfN*	240	139	0.58	15.9	16.2	16.5	2.8	3.3	TaN*	337	247	0.73	32.0	32.0	30.5	4.3	6.1	WN*	374	144	0.39	9.0	10.5	21.0	3.4	5.3
	253 ^c	137 ^c	0.54 ^c							384 ^c	261 ^c	0.68 ^c							349 ^c	148 ^c	0.42 ^c					
										318 ^a	213 ^a	0.67 ^a							376 ^b	157 ^b	0.42 ^b					

^aCalculation⁵³, ^bCalculation⁵⁴, ^cCalculation⁵⁵, ^dCalculation⁵⁶,
^eExperiment⁵⁷, ^fCalculation⁵⁸.

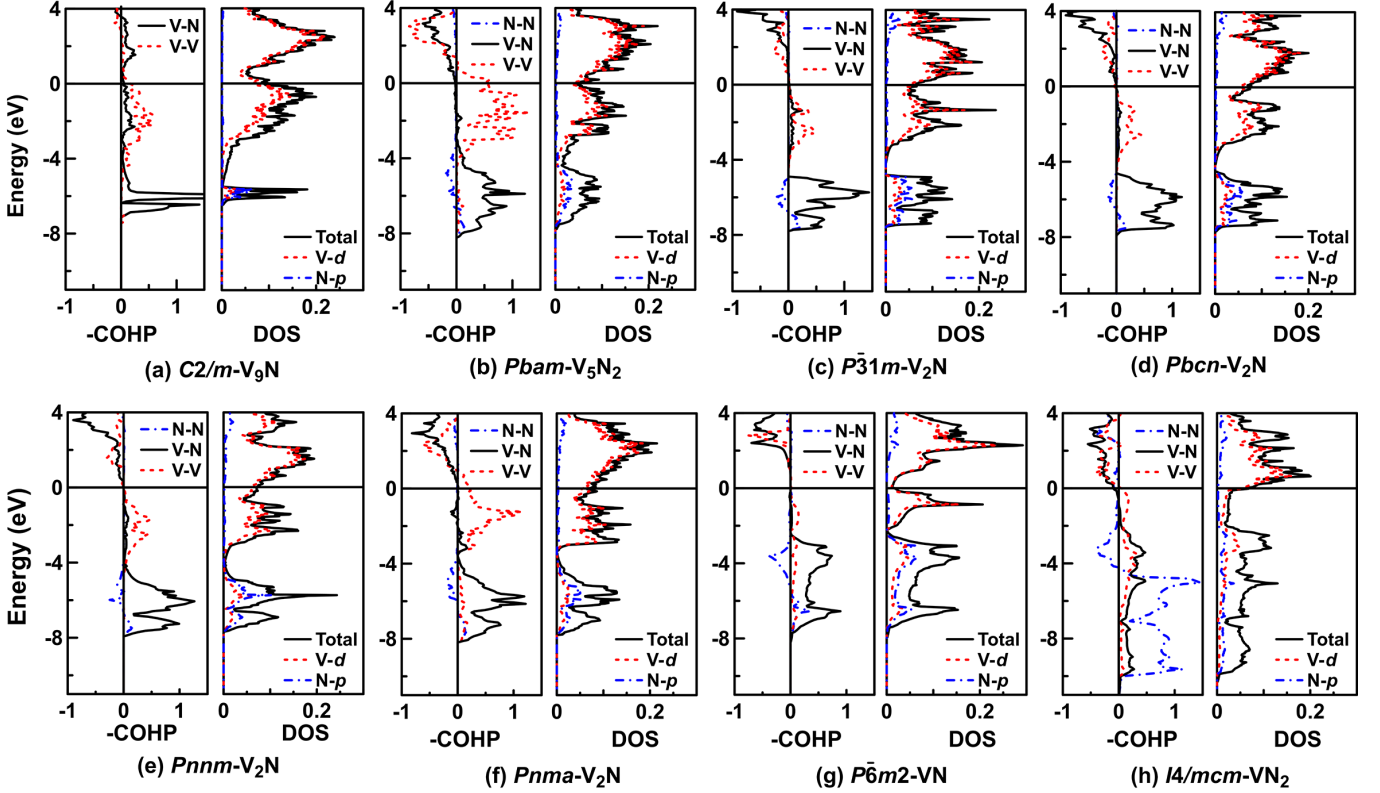


FIG. 8: (Color online) Total DOS, projected DOS and crystal orbital Hamilton population (-COHP) curves for V-N compounds at 0 GPa. Bonding and antibonding correspond to positive and negative values of -COHP, respectively.

tween the V-d and N-p states. Crystal orbital Hamilton population (COHP) is often used to identify the bonding or anti-bonding character of interatomic interactions in a crystal. The calculated -COHP [Fig. 8] of vanadium subnitrides is characterized by massively V-V and V-N bonding states and minor anti-bonding states between N-N below the Fermi level. It should be pointed out that there is no N-N interaction in $C2/m-V_9N$ due to the absence of direct atomic contacts between N atoms. With the increase of the nitrogen content, the bonding NN interactions in $I4/mcm-VN_2$ become strong (as revealed

by the positive ICOHP values) although with small N-N antibonding regions around -3.5 eV [Fig. 8(h)], which, together with the V-V and V-N bonding states below the Fermi level, greatly enhance the mechanical properties. Compared with other V-N compounds, the large overlap between V-d and N-p is shown in the projected DOS of WC-type VN. Meanwhile, the -COHP reveals a strong V-N covalent bonding between the V and N (-ICOHP is 2.7 eV/pair for the nearest V-N) and in addition some V-V bonding component [Fig. 8(g)]. Both evidences correspond to a strong V-N bond in WC-type

VN, contributing to its good mechanical properties.

IV. CONCLUSIONS

Stable V-N compounds and their crystal structures at pressures up to 120 GPa have been predicated using *ab initio* evolutionary algorithm USPEX. Four new phases $C2/m$ -V₉N, $Pbam$ -V₅N₂, $Pnma$ -V₂N and $I4/mcm$ -VN₂ are reported. All the predicted high-pressure vanadium nitrides can be theoretically preserved as metastable phases at zero pressure since they are all dynamically stable at zero pressure. The sequence of phases of V₂N under pressure is ε -Fe₂N-type V₂N \rightarrow ζ -Fe₂N-type V₂N \rightarrow Fe₂C-type V₂N \rightarrow $Pnma$ -V₂N. In addition, the enthalpy and lattice dynamics properties of several vanadium mononitride are analyzed. It is expected WC-type VN can be synthesized under high pressure. Structural features, relative stabilities, mechanical properties, electronic structures and chemical bonding of all the V-N

compounds are systematically analyzed at 0 GPa. WC-type VN has the superior Vickers hardness (~ 37 GPa) and fracture toughness (4.3-6.1 MPa m^{1/2}) which mainly originate from its strong V-N bonding. Another new high-pressure phase $I4/mcm$ -VN₂ also exhibits high bulk modulus (311 GPa), high shear modulus (214 GPa), Vickers hardness (24.8-26.9 GPa) and fracture toughness (3.6-6.6 MPa m^{1/2}). Hardness and fracture toughness are determined both by the strength and topology of bond networks.

V. ACKNOWLEDGMENTS

Calculations were carried out the Extreme Science and Engineering Discovery Environment (XSEDE), which is supported by National Science Foundation grant number ACI-1053575. A.R.O. thanks Russian Science Foundation (grant 19-72-30043).

-
- * Electronic address: zhangjin225@gmail.com
 † Electronic address: a.ogonov@skoltech.ru
- ¹ G. Farges, E. Beauprez, and M. Sainte Catherine, *Surf. Coat. Tech.* **61**, 238 (1993).
 - ² R. Sanjinés, P. Hones, and F. Lévy, *Thin Solid Films* **332**, 225 (1998).
 - ³ W. Rostoker and A. Yamamoto, *Trans. Am. Soc. Met.* **46**, 1136 (1954).
 - ⁴ C. Escobar, J. Caicedo, and W. Aperador, *J. Phys. Chem. Solids* **75**, 23 (2014).
 - ⁵ U. Wiklund, B. Casas, and N. Stavlid, *Wear* **261**, 2 (2006).
 - ⁶ M. Fallqvist and M. Olsson, *Wear* **297**, 1111 (2013).
 - ⁷ K. Kutschej, B. Rashkova, J. Shen, D. Edwards, C. Mitterer, and G. Dehm, *Thin Solid Films* **516**, 369 (2007).
 - ⁸ J. Caicedo, G. Zambrano, W. Aperador, L. Escobar-Alarcon, and E. Camps, *Appl. Surf. Sci.* **258**, 312 (2011).
 - ⁹ D. Choi, G. E. Blomgren, and P. N. Kumta, *Adv. Mater.* **18**, 1178 (2006).
 - ¹⁰ O. Carlson, J. Smith, and R. Nafziger, *Metall. Mater. Trans. A* **17**, 1647 (1986).
 - ¹¹ T. Onozuka, *J. Appl. Crystallogr.* **11**, 132 (1978).
 - ¹² D. I. Potter, H. D. Epstein, and B. M. Goldstein, *Metall. Trans.* **5**, 2075 (1974).
 - ¹³ G. Nouet, J. Vicens, and P. Delavignette, *Phys. Status Solidi A* **62**, 449 (1980).
 - ¹⁴ F. Kubel, W. Lengauer, K. Yvon, K. Knorr, and A. Junod, *Phys. Rev. B* **38**, 12908 (1988).
 - ¹⁵ W. Weber, P. Roedhammer, L. Pintschovius, W. Reichardt, F. Gompf, and A. Christensen, *Phys. Rev. Lett.* **43**, 868 (1979).
 - ¹⁶ E. I. Isaev, S. I. Simak, I. Abrikosov, R. Ahuja, Y. K. Vekilov, M. Katsnelson, A. Lichtenstein, and B. Johansson, *J. Appl. Phys.* **101**, 123519 (2007).
 - ¹⁷ V. Ivashchenko and P. Turchi, *Phys. Rev. B* **78**, 224113 (2008).
 - ¹⁸ C. Ravi, *Calphad* **33**, 469 (2009).
 - ¹⁹ V. Ivashchenko, P. Turchi, V. Shevchenko, and E. Olifan, *Phys. Rev. B* **84**, 174108 (2011).
 - ²⁰ C. Ravi, H. Sahu, M. Valsakumar, and A. van de Walle, *Phys. Rev. B* **81**, 104111 (2010).
 - ²¹ A. Mei, O. Hellman, N. Wireklint, C. Schlepuetz, D. Sangiovanni, B. Alling, A. Rockett, L. Hultman, I. Petrov, and J. E. Greene, *Phys. Rev. B* **91**, 054101 (2015).
 - ²² L. Toth, *Transition metal carbides and nitrides* (Elsevier, 2014).
 - ²³ H. O. Pierson, *Handbook of Refractory Carbides & Nitrides: Properties, Characteristics, Processing and Apps.* (William Andrew, 1996).
 - ²⁴ A. R. Oganov and C. W. Glass, *J. Chem. Phys.* **124**, 244704 (2006).
 - ²⁵ A. O. Lyakhov, A. R. Oganov, H. T. Stokes, and Q. Zhu, *Comput. Phys. Commun.* **184**, 1172 (2013).
 - ²⁶ A. R. Oganov, A. O. Lyakhov, and M. Valle, *Acc. Chem. Res.* **44**, 227 (2011).
 - ²⁷ J. P. Perdew, K. Burke, and M. Ernzerhof, *Phys. Rev. Lett.* **77**, 3865 (1996).
 - ²⁸ G. Kresse and J. Furthmüller, *Phys. Rev. B* **54**, 11169 (1996).
 - ²⁹ M. Chase, *AIP* (1998).
 - ³⁰ P. E. Blöchl, *Phys. Rev. B* **50**, 17953 (1994).
 - ³¹ A. Togo, F. Oba, and I. Tanaka, *Phys. Rev. B* **78**, 134106 (2008).
 - ³² X.-Q. Chen, H. Niu, D. Li, and Y. Li, *Intermetallics* **19**, 1275 (2011).
 - ³³ Y. Tian, B. Xu, and Z. Zhao, *Int. J. Refract. Met. Hard Mater.* **33**, 93 (2012).
 - ³⁴ E. Mazhnik and A. R. Oganov, *Journal of Applied Physics* **126**, 125109 (2019).
 - ³⁵ H. Niu, S. Niu, and A. R. Oganov, *J. Appl. Phys.* **125**, 065105 (2019).
 - ³⁶ G. Krier, O. Jepsen, A. Burkhardt, and O. Andersen, *Stuttgart, April* (1995).
 - ³⁷ H. Hahn, *Z. Anorg. Allg. Chem.* **258**, 58 (1949).
 - ³⁸ A. N. Christensen and B. Lebeck, *Acta Crystallogr., Sect. B: Struct. Sci* **35**, 2677 (1979).
 - ³⁹ P. Chun-Ying, Z. Da-Wei, B. Dai-Xiao, L. Cheng, J. Xi-

- Lian, S. Tai-Chao, and Z. Fei-Wu, *Chin. Phys. B* **23**, 026201 (2014).
- ⁴⁰ D. Palmer, “Crystalmaker,” (2007).
- ⁴¹ S. Yu, Q. Zeng, A. R. Oganov, G. Frapper, and L. Zhang, *Physical Chemistry Chemical Physics* **17**, 11763 (2015).
- ⁴² P. Mohn, *J. Phys. C: Solid State Physics* **21**, 2841 (1988).
- ⁴³ A. Friedrich, B. Winkler, E. A. Juarez-Arellano, and L. Bayarjargal, *Materials* **4**, 1648 (2011).
- ⁴⁴ P. Vajeeston, P. Ravindran, C. Ravi, and R. Asokamani, *Phys. Rev. B* **63**, 045115 (2001).
- ⁴⁵ J. Nye, *Physical Properties of Crystals: Their Representation by Tensors and Matrices*, Oxford science publications (Clarendon Press, Oxford, 1985).
- ⁴⁶ Y. Liang, X. Yuan, and W. Zhang, *Solid State Commun.* **150**, 2045 (2010).
- ⁴⁷ S. Wang, X. Yu, J. Zhang, L. Wang, K. Leinenweber, D. He, and Y. Zhao, *Crystal Growth & Design* **16**, 351 (2016).
- ⁴⁸ I. Frantsevich, F. Voronov, S. Bokuta, and I. Frantsevich, *Naukova Dumka, Kiev*, 60 (1983).
- ⁴⁹ V. V. Brazhkin, A. G. Lyapin, and R. J. Hemley, *Philos. Mag. A* **82**, 231 (2002).
- ⁵⁰ S. Pugh, *Philos. Mag.* **45**, 823 (1954).
- ⁵¹ V. Ivashchenko, P. Turchi, and E. Olifan, *Phys. Rev. B* **82**, 054109 (2010).
- ⁵² Z. Zhao, K. Bao, F. Tian, D. Duan, B. Liu, and T. Cui, *Phys. Chem. Chem. Phys.* **17**, 22837 (2015).
- ⁵³ J. Li, X. Wang, K. Liu, D. Li, and L. Chen, *J. Superhard Mater.* **33**, 173 (2011).
- ⁵⁴ L. Song and Y.-X. Wang, *Phys. Status Solidi B* **247**, 54 (2010).
- ⁵⁵ E. Zhao and Z. Wu, *J. Solid State Chem.* **181**, 2814 (2008).
- ⁵⁶ E. Zhao, J. Wang, J. Meng, and Z. Wu, *Comput. Mater. Sci* **47**, 1064 (2010).
- ⁵⁷ A. Y. Ganin, L. Kienle, and G. V. Vajenine, *J. Solid State Chem.* **179**, 2339 (2006).
- ⁵⁸ Z. Ming and K.-H. Wang, *Mod. Phys. Lett. B* **29**, 1550009 (2015).
- ⁵⁹ P. Ravindran, L. Fast, P. A. Korzhavyi, B. Johansson, J. Wills, and O. Eriksson, *J. Appl. Phys.* **84**, 4891 (1998).